Experimental and Computational Investigation of a Small-Scale Vertical Axis Wind Turbine with Dynamic Blade Pitching

Moble Benedict *
Department of Aerospace Engineering, Texas A and M University, College Station, TX, 77843
Vinod Lakshminarayan †
Science and Technology Corporation, Ames Research Center, Moffett Field, CA, 94035
Jeremy Garber ‡ Inderjit Chopra §
Alfred Gessow Rotorcraft Center, University of Maryland, College Park, MD, 20742

ABSTRACT

This paper describes the systematic performance measurements and computational (CFD) studies conducted to investigate the performance of a small-scale dynamic-pitch vertical axis wind turbine (VAWT). The VAWT prototype was built and tested in a wind tunnel to understand the role of blade-pitch kinematics and flow curvature effects on turbine aerodynamic efficiency. The three parameters investigated in the experimental study were blade pitching amplitude (symmetric pitching), asymmetry in pitch kinematics between frontal and rear halves, and blade chord (or chord/radius ratio). Even though the optimal pitch amplitude is dependent on the tip speed ratio (TSR), moderate pitch amplitudes ($\pm$ 20°) had the highest overall efficiency for the symmetric pitch cases. The tip speed ratio corresponding to the maximum C_P decreased with increasing pitch amplitudes. The TSR corresponding to maximum C_P for 20° pitch amplitude was around 1.4, while the optimal TSR for the 40° case was around 0.7. Because of the differences in the flow velocities in the front and rear halves, for maximizing power extraction, the pitch angles required in the front is significantly higher than that in the rear. The optimal performance of the turbine occurred at a phasing of 0°. However, the performance was observed to be forgiving for small changes in phasing (<10°) in the positive direction (phase-lead), however, not in the negative direction. Increasing the chord/radius from 0.19 to 0.25 caused significant improvements in turbine efficiency especially at higher pitch amplitudes because of the flow curvature effects. A CFD model was developed and extensively validated with the present experimental data. The validated CFD model was used to understand the effect of the different parameters on turbine performance by analyzing the blade aerodynamics at various azimuthal locations. CFD analysis showed that the blade extracts most of the power in the frontal half of its circular trajectory and in some cases even lose power in the rear half. This study clearly indicates the potential for major improvements in VAWT performance with novel blade kinematics, optimal chord/radius ratio, and using cambered blades.

Nomenclature

A	Turbine frontal area, $b \times D$
b	Blade span
c	Blade chord
C_P	Coefficient of power
D	Turbine diameter
R	Turbine radius
TSR	Tip speed ratio, $\Omega R/U_{inf}$
U_{inf}	Wind speed
Ω	Rotational speed of the turbine
Ψ	Azimuthal location
ϕ	Blade pitch phasing
ρ	Air density, 1.225 Kg/m^3
θ	Blade pitch angle

*email:<benedict@tamu.edu>
†email:<vinod.k.lakshminarayan.ctr@mail.mil>
‡email:<jgarber2@umd.edu>
§email:<chopra@umd.edu>
Presented at the 71st American Helicopter Society Annual Forum, Virginia Beach, VA, May 5–7, 2015.

Figure 1: **Optimized fixed-pitch VAWT farm developed by California Insitute of Technology [2].**

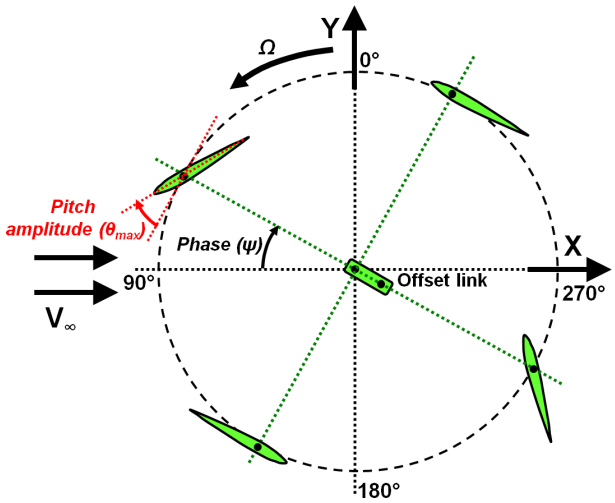

Figure 2: **Blade pitch kinematics and defintion of coordinate system on a dynamic-pitch VAWT.**

INTRODUCTION

With increasing energy costs, rapid depletion of fossil fuels and growing concerns about the environmental effects of burning hydrocarbons, researchers have been looking at alternate, more environmentally benign sources to create power. Wind power, a renewable and virtually inexhaustible power source, is a promising means of green energy production. However, at present, horizontal axis wind turbines are the most established method of harvesting wind energy. Majority of the wind energy plants today, are in the form of windmill farms having several mega-Watt capacity, comprising of large horizontal axis windmills (rated at several 100 kWs) driving electric generators and feeding into power supply grids. A major deterrent to the continued development of wind energy at remote sites is the limited capacity of the nation's electricity distribution grid. Therefore, there is a strong need to co-locate energy generation based on the demand in order to reduce the load and losses in the grid system [1]. Because large cities are the biggest consumers of electricity, it is necessary to design small scale (1-2 kW peak power), efficient, stand-alone wind turbines to meet their growing energy demand. However, unlike the large open windmill farms, extracting wind energy in an urban scenario is challenging because of the tight space constraints and the fact that wind profile is highly turbulent with rapid fluctuations, both in terms of magnitude as well as direction.

In an urban scenario, where space is of the essence, an important criterion for choosing one wind turbine concept over the other for a small windmill farm, would be the power extracted per unit ground area (also known as power density). HAWTs are not very attractive for such a scenario because of their need to maintain a significant lateral (3 – 5 turbine diameters in cross-wind direction) and longitudinal (6 – 10 diameters in downwind direction) separation between adjacent turbines and therefore would have a large footprint, or in other words, very low power density ($2 - 3\ W/m^2$). However, previous studies have shown that vertical axis wind turbines (VAWTs) could have very close wind turbine spacing, and if placed appropriately in a farm (as shown in Fig. 1), it could greatly enhance the farm efficiency ($\approx 30\ W/m^2$, which is almost ten times more power extracted per unit land area compared to HAWTs) because of the constructive interference between the turbines [2].

The power density of a farm would effectively depend on the lateral and longitudinal spacing between the turbines (or number of turbines per unit area) and the power density of the individual turbines itself. Therefore, it is important to examine the power density for a single turbine, which is in fact the power extracted per unit projected area. Note that, the area used for power density calculation in the case of a HAWT, is the projected circular swept area when the turbine is yawed 360° ($A = \pi R^2$). In general, the power density of a VAWT could be higher because the swept area of a VAWT (i.e., the cross-sectional area that interacts with the wind) need not be equally apportioned between its breadth, which determines the size of its footprint, and its height. By contrast, the circular sweep of HAWT blades dictates that the breadth and height of the rotor swept area are identical. Therefore, whereas increasing HAWT rotor swept area necessarily increases the turbine footprint, it is possible to increase the swept area of a VAWT independent of its footprint, by increasing the rotor blade height. Therefore, theoretically, for a VAWT, the power density could be increased indefinitely by increasing the turbine height until it encounters other

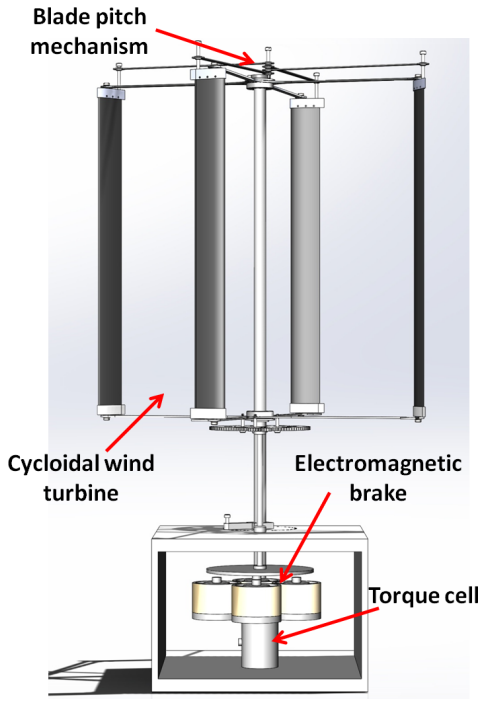

Figure 3: **Experimental setup.**

constraints which would limit its maximum height.

Even though VAWTs can have very high power densities compared to HAWTs, the reason why VAWTs never gained popularity was because most of the VAWTs built so far used fixed blade pitch angle (Fig. 1), and this configuration suffers from very low efficiency especially at low tip speed ratios (TSR) (TSR=blade speed/wind speed, $\Omega R/U_{inf}$) and are only self-starting for certain wind directions. Note that, until recently, the efficiency was the biggest concern for wind turbines and the farm power density was less of a factor, because turbines were mostly installed at remote locations where there are no space constraints. However, today, for a small-scale wind turbine to be used in an urban environment, power density is as important as the turbine efficiency. Therefore, the next generation small-scale turbines need to have not just high efficiencies, but also high power densities. Hence, a VAWT design may be a better starting point than HAWTs for the design of wind farms with high power density. However, it is important to realize that the efficiency of fixed-pitch VAWTs needs to be improved significantly.

Previous studies have shown that the efficiency of a VAWT could be improved by appropriately modulating the pitch angle of the blade (dynamic pitching) as it moves around the azimuth as shown in Fig. 2 [1, 3 – 6]. However, these studies were not comprehensive enough to fully understand the physics or optimize the performance of such a concept. Another key barrier in practically implementing such a turbine was developing a simplified blade pitch mechanism. Most of the previous studies proposed mechanisms, which were complicated (such as active blade pitching using individual blade actuators) and required significant amount of power to dynamically vary blade pitch. Other pitching mechanisms that have been developed were passive in nature, and therefore, utilized the inertial and aerodynamic forces acting on the blade to dynamically pitch the blade. Hence, the blade pitch schedule was a function of the operating conditions, leading to very low efficiencies. These are some of the reasons why such a turbine remained elusive, even though, it has the potential to achieve high efficiency (comparable to HAWTs) along with high power density. Therefore, one of the key focuses of our research was to develop a simplified, practically feasible blade pitching mechanism so that such a turbine could become a reality.

The previous VAWT research conducted by the authors included very limited experimental studies and focused primarily on utilizing a 2D CFD analysis to understand the physics of power extraction on a dynamic-pitch turbine [7]. This study clearly showed the advantages of a dynamic-pitch turbine over a fixed-pitch turbine and also showed that blade kinematics and chord/radius ratio could potentially have a significant impact on turbine efficiency. The present study is a continuation of this previous work reported in Ref. [7] and is focused on conducting systematic experiments to understand the effects of the different blade kinematic parameters and chord/radius ratio on power extraction and further, use a well-validated in-house CFD analysis to understand the physics of power extraction. The long-term goal of the present research is to develop a revolutionary, small-scale (diameter of ≈ 2 meters) variable pitch VAWT (1-2 kW range) with extremely high efficiency and power density to be used in urban environments such as roof-tops. The turbine should be able to be used individually or in a small farm, in which case, the optimal locations of these turbines will have to be determined. The present study is the first step towards achieving this goal. The insights gained from this study could be used to design more efficient VAWTs in the future.

VAWT Prototype and Experimental Setup

An instrumented VAWT prototype has been designed and built as shown in Fig. 3. The pitch angle of each of the blades is varied periodically as the blade moves around the azimuth using a four-bar based passive pitching mechanism, the details of which are discussed in

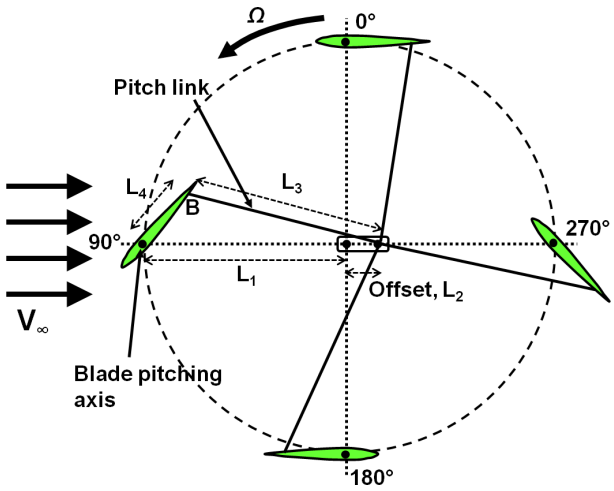

(a) Schematic showing the blade pitch mechanism.

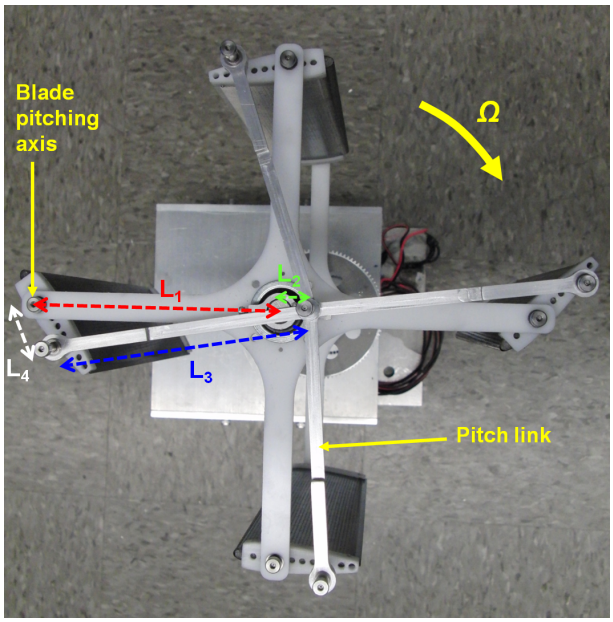

(b) Actual blade pitch mechanism on the VAWT prototype.

Figure 4: **Four-bar based blade pitch mechanism on the present dynamic-pitch VAWT prototype.**

the next section. The cyclic blade pitching kinematics is shown in Fig. 2. The present setup was designed such that the blade pitch kinematics could be easily varied. The turbine is 4-bladed and has a diameter of 13.5 inches and blade span of 10 inches. Two different sets of blades were tested with uniform blade chords of 1.3 inches and 1.7 inches, respectively with both sets utilizing NACA 0015 airfoil section. It is important for the VAWT blades to be lightweight and have a high stiffness to weight ratio to minimize bending and torsional deformations and also the structural loads at high rotational speeds. Therefore, the present blades utilized an innovative structural design, where the blades were fabricated using a single layer of carbon prepreg wrapped around a foam core and then baked inside a mold.

The entire setup was placed in front of an open-jet wind tunnel with a test-section of 22 inch by 22 inch. The rotational speed of the turbine (and hence the torque) was varied for a constant wind speed by adjusting the voltage supplied to the custom-built electromagnetic brake. The braking torque was measured using a non-rotating reaction-based torque load cell (shown in Fig. 3) and the turbine rotational speed was measured using a laser tachometer. When the turbine attains a steady rotational speed, the power generated by the turbine is calculated from the measured braking torque and rotational speed.

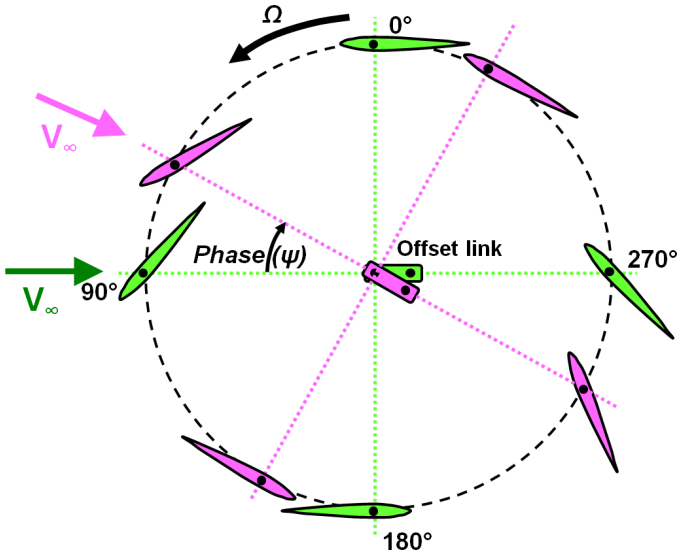

Figure 5: **Adjusting the pitch phasing by rotating the offset link to adapt to the change in wind direction.**

Pitch Mechanism Design

A simplified blade pitch changing mechanism is the key to the success of a dynamic-pitch VAWT. The previous more involved design of pitching mechanisms was the main reason why the variable pitch VAWTs became unpopular in the late 1970s, even though they were proven to be self-starting and much more efficient than their

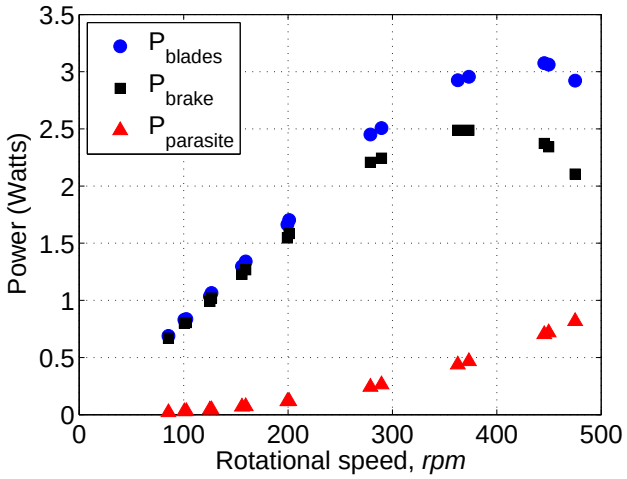

Figure 6: **Experimental results showing the variation of different components of power with turbine rotational speed.**

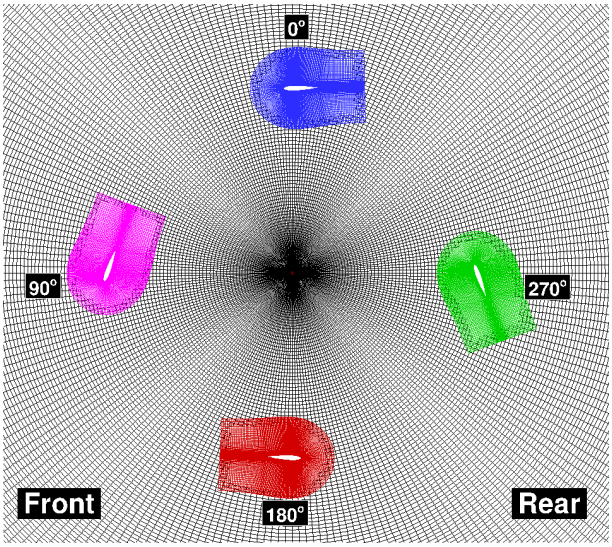

Figure 7: **CFD grid system used for the 6.75 inch radius 4-bladed cyclorotors with 1.3 inch blade chord.**

fixed pitch counterparts. Therefore, a key focus of our research was to develop a simplified blade pitch mechanism.

As shown in Fig. 4(a), the present pitching mechanism is based on a four-bar linkage system, which is designed in such a way that the blade pitches automatically in a cyclic fashion as the turbine rotates. Therefore, the only power penalty incurred in its operation is the frictional losses associated with the moving components. As shown in the schematic, L_1, L_2, L_3 and L_4 are the four linkage lengths. The key component of the pitching mechanism is the offset link of length L_2. The pitch links (of length L_3) are connected to the end of the offset link on one end and the other end is connected to point B, on the blade, which is at a distance L_4 behind the pitching axis. The connections at both ends of the pitch link are through pin joints to allow the rotational degree of freedom. The radius of the rotor forms the linkage length L_1. With this arrangement, as the rotor rotates, the blades automatically pitch, where the pitching amplitude depends on the offset length, L_2, when the other linkage lengths remain fixed. The actual pitching mechanism implemented on the VAWT prototype is shown in Fig. 4(b). The four-bar linkage system can be clearly seen in the figure.

As explained before, the magnitude of the offset (L_2) changes the blade pitching amplitude and the direction in which the offset link is pointing would change the phasing of the cyclic blade pitching as shown in Fig. 5. For the sake of simplicity, the present prototype is designed such that the offset length (L_2) could not be changed while the turbine is rotating (Fig. 4(b)), which means the blade pitch kinematics (pitch amplitude, θ_{max}) is fixed. However, as shown in Fig. 5, in the present mechanism, the offset link could be rotated to actively change the phasing of the cyclic pitch (ϕ) depending on the direction of incoming wind to maximize efficiency. This method of altering the phasing of blade pitching is instantaneous and much simpler than rotating the entire HAWT in the direction of the wind. This capability of the present VAWT pitch mechanism, to immediately respond to a change in wind direction, is the key to maximizing the power extraction in urban environments where wind direction changes rapidly.

Experimental Methodology

As explained in the previous section, the power extracted by the turbine was calculated from the measured brake torque (with the electromagnetic brake) and its rotational speed. The inherent assumption here being, once the turbine reaches steady state, the power extracted by the turbine is equal to the braking power. However, the goal of the present experiment was not to measure the net aerodynamic power output of the turbine, but, the complete power extracted by the blades, which does not include the power lost (or parasitic power) in rotating the rest of the turbine structure such as the endplates, pitch links, etc. Assuming all the power on a turbine is extracted by the blades, when the turbine reaches the equilibrium speed, the relation below should be satisfied.

$$P_{blades} = P_{brake} + P_{parasite} \quad (1)$$

where P_{blades} is the power extracted by the blades,

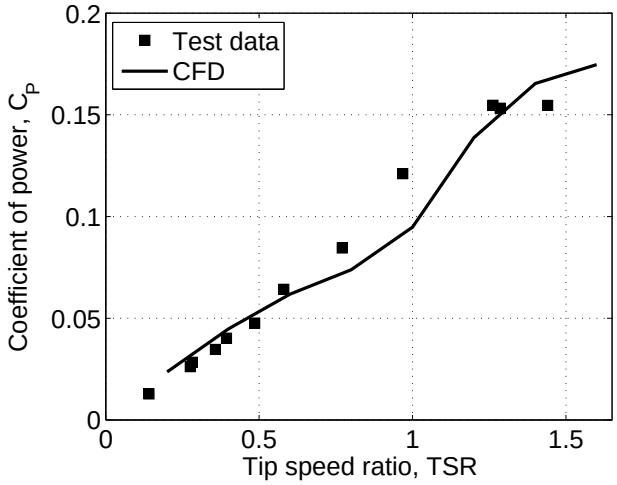

(a) Variation of coefficient of power with tip speed ratio for 15° blade pitch amplitude.

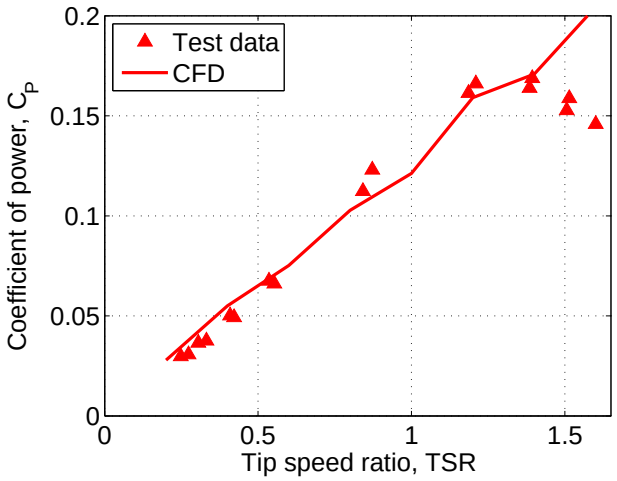

(b) Variation of coefficient of power with tip speed ratio for 20° blade pitch amplitude.

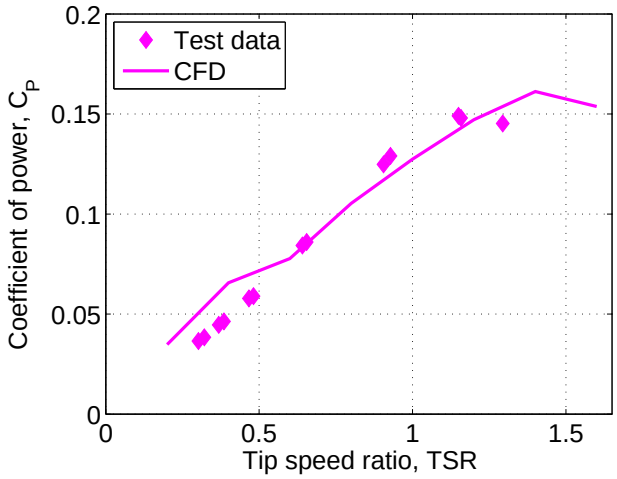

(c) Variation of coefficient of power with tip speed ratio for 25° blade pitch amplitude.

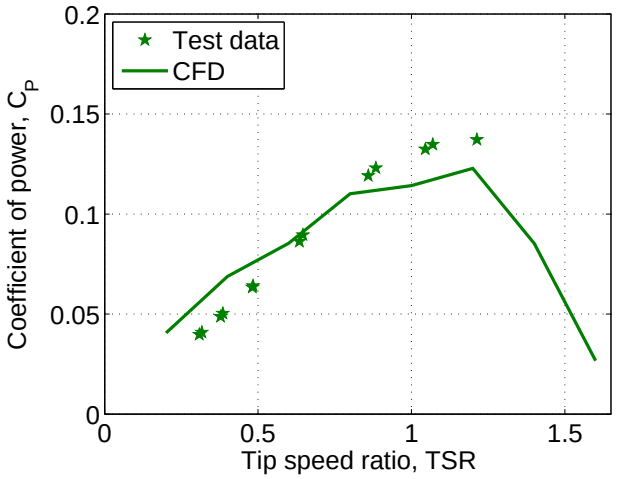

(d) Variation of coefficient of power with tip speed ratio for 30° blade pitch amplitude.

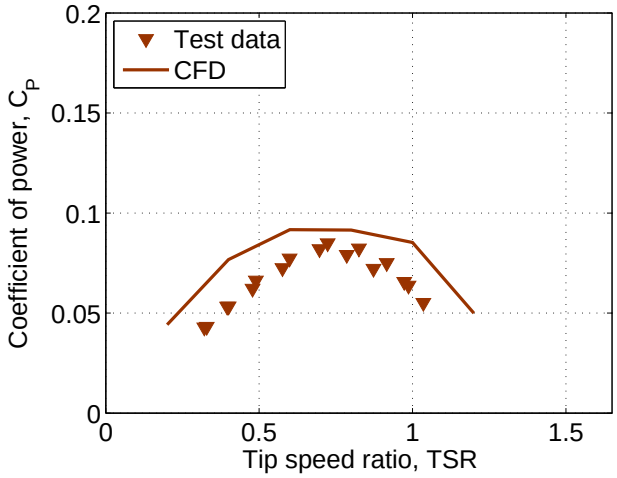

(e) Variation of coefficient of power with tip speed ratio for 35° blade pitch amplitude.

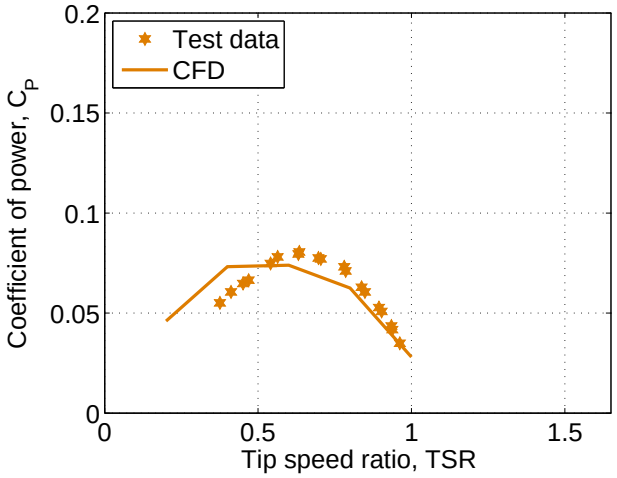

(f) Variation of coefficient of power with tip speed ratio for 40° blade pitch amplitude.

Figure 8: **Validation of 2D CFD results with the experimental data obtained for 15°, 20°, 25°, 30°, 35° and 40° blade pitching amplitudes (blade chord = 1.3 inches, wind speed = 7 m/s).**

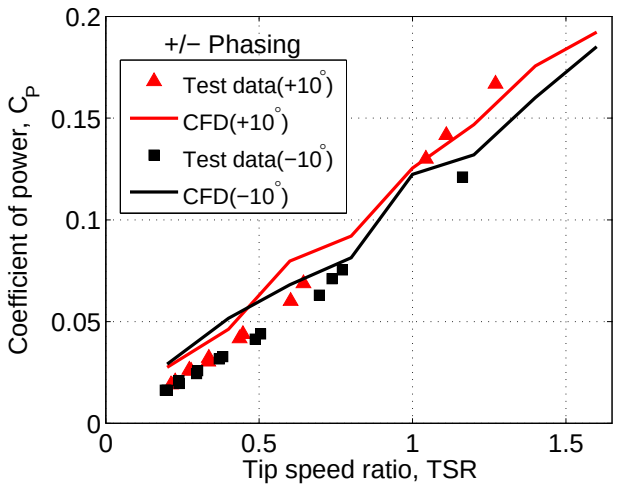

(a) Variation of coefficient of power with tip speed ratio for 20° blade pitch amplitude and ±10° phasing.

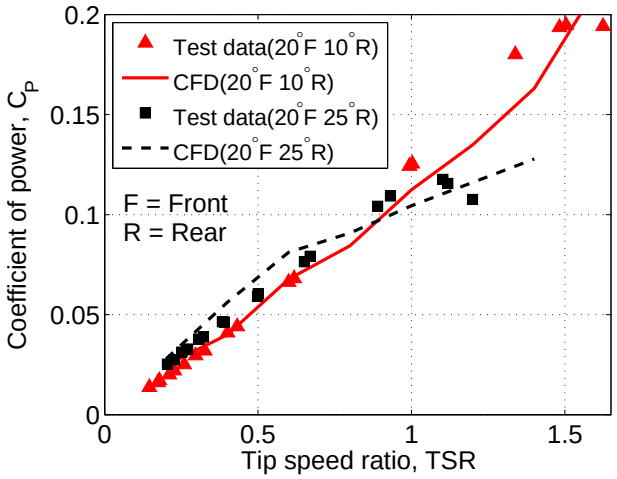

(b) Variation of coefficient of power with tip speed ratio for two asymmetric pitching cases with 20° blade pitch in the front, 10° and 25° in rear.

Figure 9: **Validation of 2D CFD results with the experimental data obtained for non-zero phasings and asymmetric pitching (blade chord = 1.3 inches, wind speed = 7 m/s).**

P_{brake} is the braking power, which is also the measured power and $P_{parasite}$ is the parasitic power required to rotate the rest of the rotor structure (excluding blades), which could also include the frictional loses. This relation (Eqn. 1) shows that the measured power (P_{brake}) is not equal to the power extracted by the blades, unless the parasitic power is negligible. Therefore, tare tests were conducted in the wind tunnel by rotating rest of the turbine structure (excluding blades), using a motor at the exact same operating conditions (wind speed = 7 m/s and equilibrium rotational speeds) where each of the turbine power measurements were taken. The motor power is measured in these experiments from the motor torque (obtained using a separate torque sensor) and its rotating speed. The measured motor power is essentially the parasitic power (or tare power) required to rotate the turbine structure. Then, this parasitic power ($P_{parasite}$) was added to the previously measured brake power (P_{brake}) to obtain the total aerodynamic power extracted by just the blades (P_{blades}) (Eqn. 1). The measured varation of different components of power as a function of turbine rotational speed is shown in Fig. 6. The parasitic power, as expected, varies as the cube of turbine rotational speed. Therefore, to minimize parasitic loses, it is important to extract the maximum power at as low a tip speed ratio (TSR) as possible. It should also be noted that the present turbine design is aerodynamically much more cleaner than our previous design [7], where the parasitic power was almost the same order as brake power even at lower rotational speeds, which means a significant portion of the power extracted by the blades is lost in rotating the rest of the turbine structure.

If the tare power was not added to the brake power, the measurements would still be useful, because it would be an indicator of the complete system aerodynamic efficiency. However, such measurements would be very specific to this particular turbine because the rest of the turbine structure could change from one experimental setup to another. Also, the results from these experiments need to be used for validating lower-order aerodynamic models or CFD models, which in most cases would not be able to simulate the rest of the rotor structure, pitch-links, etc. This would not be an issue while testing a conventional HAWT because the parasitic power associated with turbine hub is negligible compared to the power extracted by the blades.

2D CFD Methodology

A 2-D CFD study was also conducted to understand the flow physics of a variable-pitch turbine. CFD simulations were performed for the same turbine geometry used in the experimental study at different blade kinematics, blade chord and tip speed ratios. The details of the flow solver and grid system used in the present study are given below.

Flow Solver

2-D simulations of the VAWT were undertaken using a compressible structured overset RANS solver, OVERTURNS [8]. This overset structured mesh solver uses

the diagonal form of the implicit approximate factorization method developed by Pulliam and Chaussee [9] with a preconditioned dual-time scheme to solve the compressible RANS equations. Computations are performed in the inertial frame in a time-accurate manner. A third-order MUSCL scheme [10] with Roe flux difference splitting [11] and Koren's limiter [12] is used to compute the inviscid terms, and second-order central differencing is used for the viscous terms. Due to the relatively low Mach numbers in which the present turbine operate, the inclusion of a low Mach preconditioner based on Turkel's [13] method accelerates the convergence and ensures accuracy of the solution. Spalart-Allmaras [14] turbulence model is employed for RANS closure. This one-equation model has the advantages of ease of implementation, computational efficiency and numerical stability.

Grid System

An overset system of meshes, consisting of C-type airfoil mesh for each blade and a cylindrical background mesh, is used for the computation. The airfoil meshes have 255×55 grid points in the wraparound and normal directions, respectively. The background cylindrical mesh has 245×221 points in the azimuthal and radial directions, respectively. Implicit hole-cutting method developed by Lee [15] and refined by Lakshminarayan [8] is used to find the connectivity information between the overset meshes. Figure 7 shows the mesh system used for the present turbine. In these figures, only the field points (points where the flow equations are solved) are shown. All the points that are blanked out either receive information from another mesh or lies inside a solid body and therefore, does not have a valid solution.

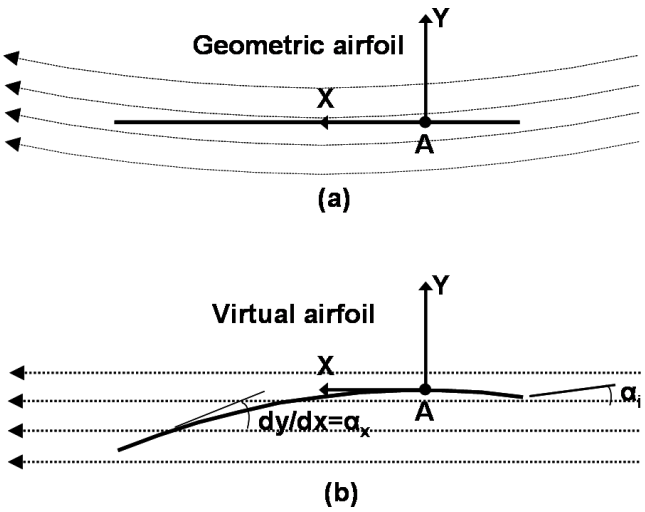

(a) Virtual camber and incidence in a curvilinear flow.

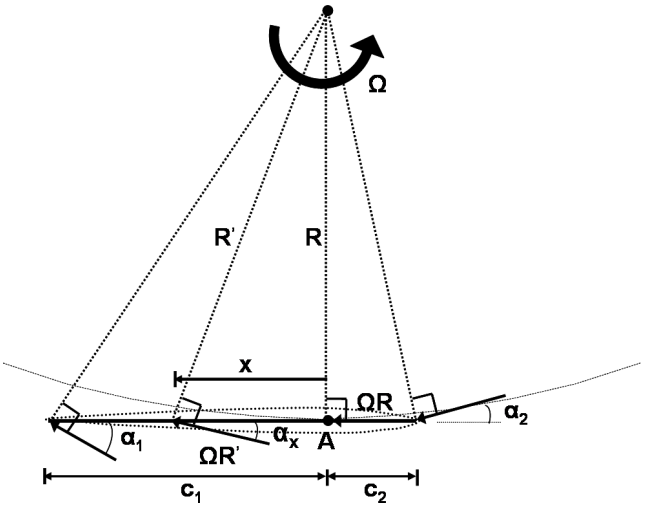

(b) Schematic explaining virtual camber.

Figure 10: **Schematic explaining virtual camber and incidence (flow curvature) effects.**

Results

For a fixed turbine geometry, the key parameters that can significantly affect power extraction on a dynamic-pitch VAWT are blade kinematics and its phasing with respect to the wind direction (ϕ, shown in Fig. 2). Two types of blade kinematics were investigated, which are symmetric and asymmetric blade pitch kinematics. In symmetric pitch kinematics the blades have the same pitch angle variation in the frontal and rear halves and the parameter that is varied is blade pitch amplitude (θ_{max}, Fig. 2). Pitch amplitude was varied from $\pm 10^\circ$ to $\pm 40^\circ$ in steps of 5° with pitching axis at the quarter chord. Asymmetric blade kinematics would involve blades having dissimilar pitch angle variation in the two halves of its circular trajectory. For the different asymmetric cases tested, the front half pitch schedule was kept constant and the rear pitch kinematics was varied in order to improve power extraction in the rear half. The other parameter that is varied is the blade chord for a fixed turbine radius to understand the effect of chord/radius on turbine performance. Each parameter was tested over a range of tip speed ratios (ratio of blade speed to wind speed, $TSR = \Omega R/U_{inf}$). Tip speed ratio was varied from around 0.3 (turbine rpm = 98) up to 1.6 (rpm = 523) for both experimental and CFD studies by changing the turbine rotational speed and keeping the wind speed fixed at 7 m/s. The wind speed was kept fixed so that the average chord-based Reynolds number would stay the same, which was around 15,000 for 1.3 inch blade chord and 20,000 for 1.7 inch chord.

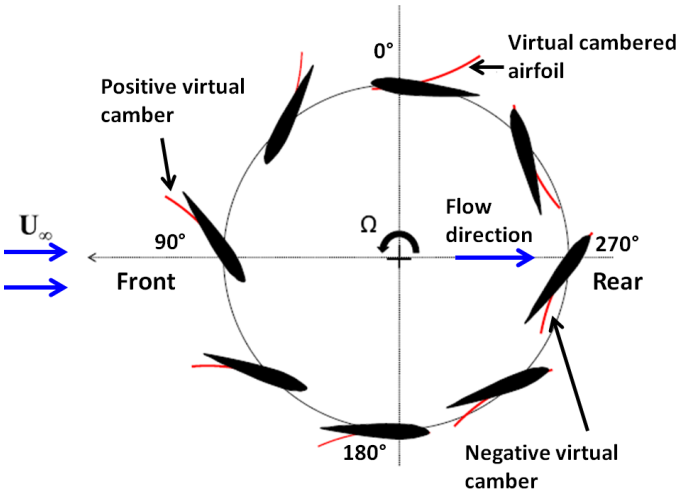

Figure 11: **Schematic showing the virtual camber and incidence on a dynamic-pitch VAWT blade at different azimuthal locations.**

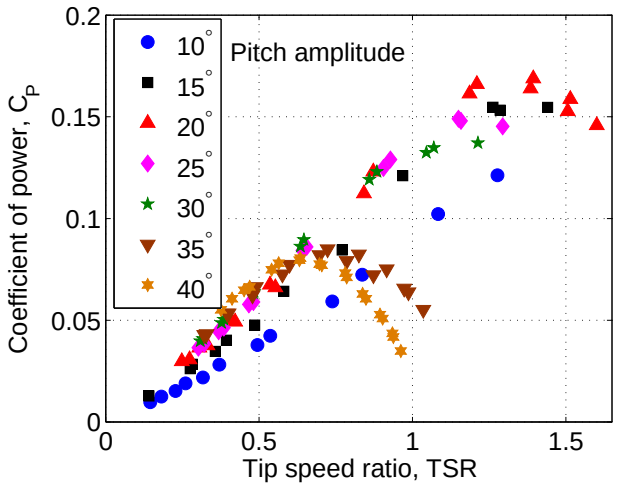

Figure 12: **Experimental results showing the variation of coefficient of power (C_P) with tip speed ratio (TSR) for 10°, 15°, 20°, 25°, 30°, 35° and 40° blade pitch amplitudes (blade chord = 1.3 inches, wind speed = 7 m/s).**

CFD Validation

Only time averaged performance from all the four blades were measured in the wind tunnel tests. Therefore, even though the experiments are useful in understanding the average performance of the turbine and how it changes with different parameters, it would not shed any light on the aerodynamics of each blade as it moves around the azimuth and how exactly is the power being extracted on such a turbine. This is the motivation for developing the present CFD analysis. However, before the CFD model could be used for understanding the physics, it should be validated with the test data. Figures 8 and 9 shows the comparison of the CFD predicted C_P values with the present test data for a range of cases. C_P is ratio of the actual power extracted by the turbine to the total ideal aerodynamic power going into the turbine and is given by Eqn. 2.

$$C_P = \frac{P_{blades}}{0.5\rho A U_{inf}^3} \tag{2}$$

where P_{blades} is the total power extracted by the blades (Eqn. 1) and A ($b \times D$) is the frontal area of the turbine.

Figure 8 shows the variation of both CFD predicted and experimentally measured coefficient of power (C_P) as a function of tip speed ratio (TSR) for ±15°, ±20°, ±25°, ±30°, ±35° and ±40° blade pitch amplitudes at 0° phasing. It can be seen that there is good correlation for most of the cases except for the 35° pitch amplitude. Figure 9 shows good correlation between CFD and experiment even for non-zero phasings and asymmetric pitch kinematics. Also, the trends predicted by CFD is very similar to that of experiments. Once the model is systematically validated, it could be used to further investigate the effect of each of these parameters as observed from the experiments. However, before that, it is essential to introduce the idea of virtual camber and incidence effects (flow curvature effects) experienced by the turbine blades as they move along a circular trajectory. Flow curvature effects play a significant role in the instantaneous aerodynamic forces experienced by the blade especially when the chord to radius is high.

Flow Curvature Effects (Virtual Camber and Incidence Effects)

Virtual camber/incidence effect is an aerodynamic phenomenon that would occur when the blades undergo an orbital motion and therefore experience a curvilinear flow [16, 17]. Blades subjected to a curvilinear flow behave very differently compared to being immersed in a rectilinear flow (Fig. 10(a)). In a curvilinear flow, the local velocity and angle of attack of the blade are unique at different locations on the chord. Because of this, a symmetric blade at 0° pitch angle in a curvilinear flow can be viewed to behave like a cambered blade at an angle of incidence (α_i) in a rectilinear flow (Fig. 10(a)). This effect will be more pronounced with VAWTs having large chord-to-radius ratio (c/R).

The virtual camber effect is clearly explained using Fig. 10(b) which shows a symmetric airfoil at a pitch angle of 0° at the bottom-most point of the blade trajectory. Point A is the pitching axis of the blade. For the sake of explanation, resultant velocity at any location on the blade chord is assumed a function of the rota-

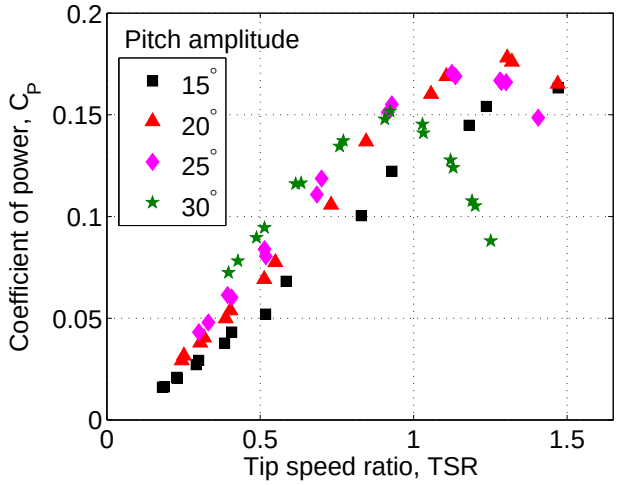

Figure 13: **Experimental results showing the variation of coefficient of power (C_P) with tip speed ratio (TSR) for 15°, 20°, 25° and 30° blade pitch amplitudes (blade chord = 1.7 inches, wind speed = 7 m/s).**

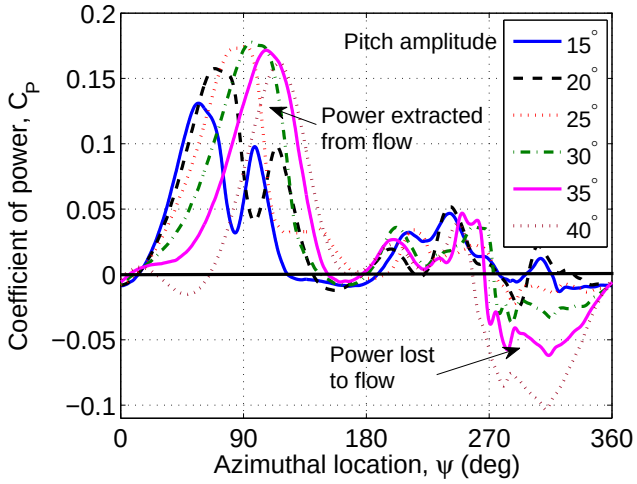

Figure 14: **Variation of coefficient of power (C_P) for one blade as it goes around the azimuth for 10°, 15°, 20°, 25°, 30°, 35° and 40° blade pitch amplitudes obtained using CFD at TSR=1.0 (positive C_P denotes power extraction and negative C_P is power lost to the flow).**

tional speed only (the freestream velocity and the pitch rate effects are ignored). Thus, as shown in Fig. 10(b), the magnitude and direction of the resultant velocity varies along the chord. The angle of incidence of the flow at any arbitrary location on the chord, x, is given by $\alpha_x = tan^{-1}(x/R)$ ($\alpha_x \approx x/R$) and the velocity magnitude is given by $\Omega R'$ where $R' = \sqrt{R^2 + x^2}$.

Now this scenario is approximately equivalent to having a cambered airfoil, with the camber line slope (dy/dx) equal to α_x in a rectilinear flow of magnitude ΩR as shown in Fig. 10(a). For the present turbine, using 1.3 inch chord blades, the c/R is 0.19 and by using a linear approximation, virtual camber is about 2.3% of chord and the virtual incidence is about 2.7°. Virtual camber is directly dependent on the chord/radius ratio of the turbine and the virtual incidence depends on both the chord/radius ratio and the chordwise location of blade pitching axis, which in the present turbine is at quarter chord. Decreasing the distance of the blade pitching axis location from the leading edge increases virtual incidence for a fixed chord/radius ratio. For a pitching axis location of 50% chord from the leading edge, the virtual incidence is zero. The virtual camber on a pitching VAWT blade is illustrated in Fig. 11, which shows the virtual camber (in red) superimposed on the geometric airfoil (in black) at various azimuthal positions. In this case a large chord/radius is chosen to clearly illustrate the virtual camber and incidence. The negative virtual camber (with respect to the flow direction) in the rear half could stall the blades even at low angles of attack which could significantly reduce power capture, which would be explained the subsequent sections. However, the positive camber in the frontal half could improve power capture in the front. Although the current turbine employs symmetric airfoils, it is worth noting that geometrically cambered airfoils could potentially improve power extraction.

Experimental Results

The experimental studies focused on three key parameters which are (1) blade pitching amplitude (symmetric pitching), (2) asymmetry in pitch kinematics between frontal and rear halves, and (3) blade chord (or chord/radius ratio)

Effect of blade pitch amplitude (symmetric pitching)

The amplitude of blade pitching plays a very crucial role in the power extraction of a dynamic-pitch wind turbine. Experiments were conducted over a range of pitch amplitudes for two different blade chords with pitching axis located at the quarter chord. Figure 12 shows the variation of coefficient of power (C_P) with tip speed ratio (TSR) for 10°, 15°, 20°, 25°, 30°, 35° and 40° blade pitch amplitudes for a blade chord = 1.3 inches. As shown in the figure, the maximum C_P increases with pitch amplitude from 10° until 20° and drops when increased beyond 20°. Even though there was only a small variation in C_P in the 15° to 25° range, the efficiency

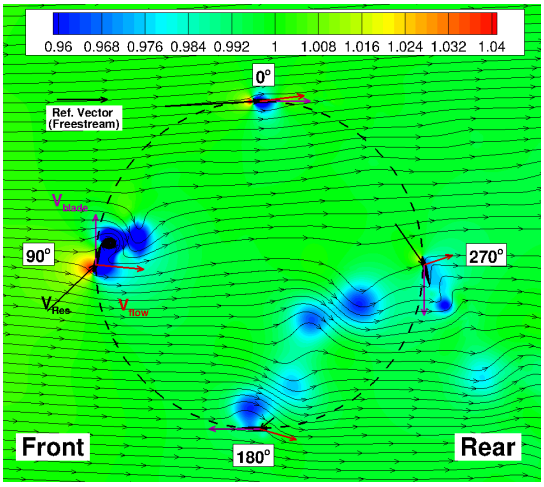

(a) Blade pitch amplitude = 15°.

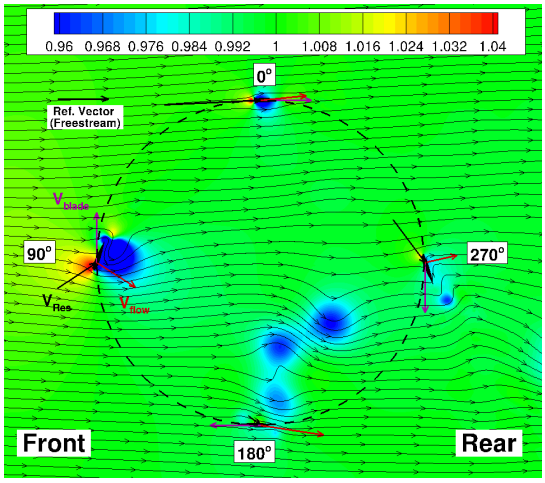

(b) Blade pitch amplitude = 20°.

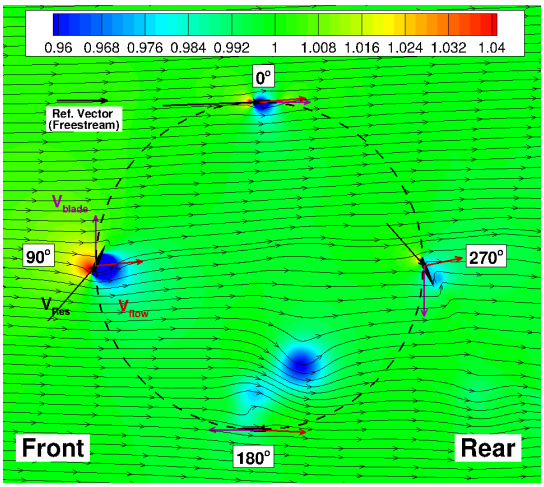

(c) Blade pitch amplitude = 25°.

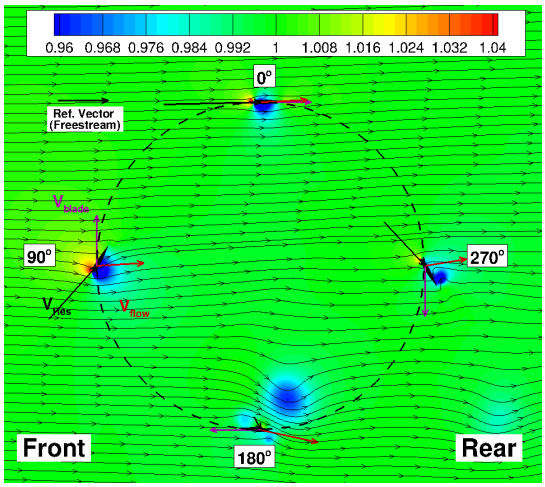

(d) Blade pitch amplitude = 30°.

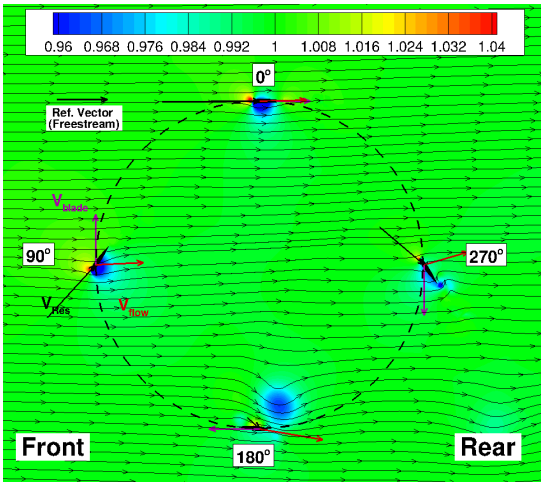

(e) Blade pitch amplitude = 35°.

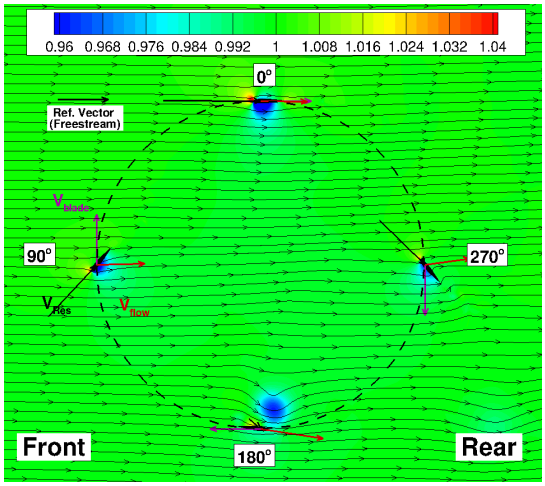

(f) Blade pitch amplitude = 40°.

Figure 15: **Physics of power extraction explained using blade aerodynamics and the CFD predicted flowfield (pressure contours with streamlines superimposed) for turbine operating at different blade pitch amplitudes at tip speed ratio (TSR) of 1 (blade chord = 1.3 inches, wind speed = 7 m/s).**

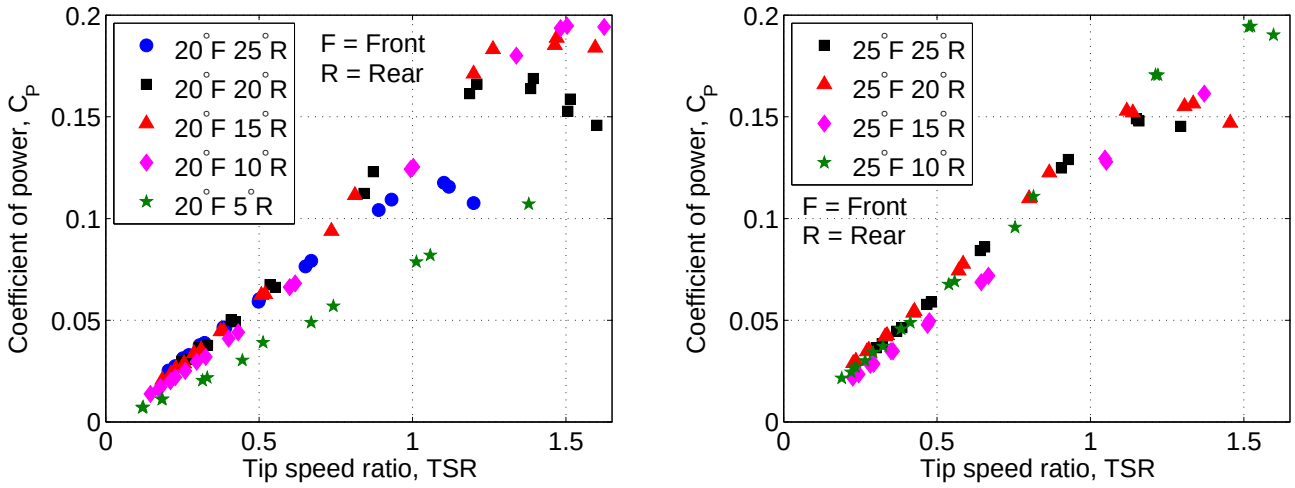

(a) Front pitch angle = 20°.

(b) Front pitch angle = 25°.

Figure 16: **Experimental results showing the variation of coefficient of power (C_P) with tip speed ratio (TSR) for two asymmetric pitching cases (blade chord = 1.3 inches, wind speed = 7 m/s).**

dropped significantly when the pitch amplitude was increased to higher values (35° and 40°). Also, it is significant to note that the tip speed ratio (TSR) corresponding to the maximum C_P decreased with increasing pitch amplitudes. The TSR corresponding to maximum C_P for 20° pitch amplitude was around 1.4, while the optimal TSR for the 40° case was around 0.7. To validate these conclusions further, pitch amplitude variation experiments were conducted with a blade chord of 1.7 inches and the results are shown in Fig. 13. Similar to the previous case, even for the 1.7 inches chord, the optimal pitch amplitude was around 20°, with 25° and 15° cases achieving slightly lower efficiency. As before, the optimal tip speed ratio decreased with increasing pitch amplitude. Also, at lower tip speed ratios (TSR<0.8), higher pitch amplitudes have better C_P. This is because at lower TSRs, because of the lower blade speed, there is more cyclic variation in angle of attack due to the free stream velocity, requiring more modulation in blade pitch angle (higher pitch amplitude) to keep the blade within the optimal operating range and also prevent it from stalling.

The validated CFD analysis was utilized to further investigate the effect of blade pitch amplitude. The first step was to use the validated CFD model to obtain the power extracted by one blade (chord = 1.3 inches) on a 4-bladed turbine as it goes around the azimuth. Figure 14 shows the variation of CFD-predicted coefficient of power (C_P) for one blade as it goes around the azimuth for 15°, 20°, 25°, 30°, 35° and 40° blade pitch amplitudes at a tip speed ratio of 1.0. In this figure, positive C_P denotes power extraction and negative C_P is power lost to the flow. It is interesting to see that the for all the pitch amplitudes, the blade extracts energy in the frontal half of the turbine (ψ=0° to ψ=180°), however, puts some of the extracted energy back into the flow in the rear half (ψ=180° to ψ=360°), especially from ψ=270° to ψ=360°. From Fig. 14, it is worth noting that the higher pitch amplitudes (30° and 35°) extract more energy in the frontal half because of the higher wind speed in the front requiring larger modulation in blade pitch angle. However, most of the extracted energy for the higher pitch amplitude is lost in the rear half because of blade stall. However, for the lower pitch amplitudes, for instance, the 20° case, even though the power extraction is lower in the frontal half, it is also able to extract a small amount of power in the rear half and thereby increasing the overall efficiency.

To understand this even further it is important to look at the flowfield predicted by CFD. However, before that, it is important to understand that the power extracted by the blade at any instant, is the product of the instantaneous tangential aerodynamic force experienced by the blade and the blade speed. If the blade is moving in the same direction as the tangential force, the power is positive or the blade is extracting power and if the blade is moving opposite to the direction of tangential force, the power is negative or the blade is losing energy into the flow. Therefore, it should be possible to explain the power variation shown in Fig. 14 by examining the aerodynamic forces experienced by the blade at different azimuthal locations. Key to obtaining the aerodynamic force is computing the resultant velocity and blade angle of attack, which could be calculated from blade kine-

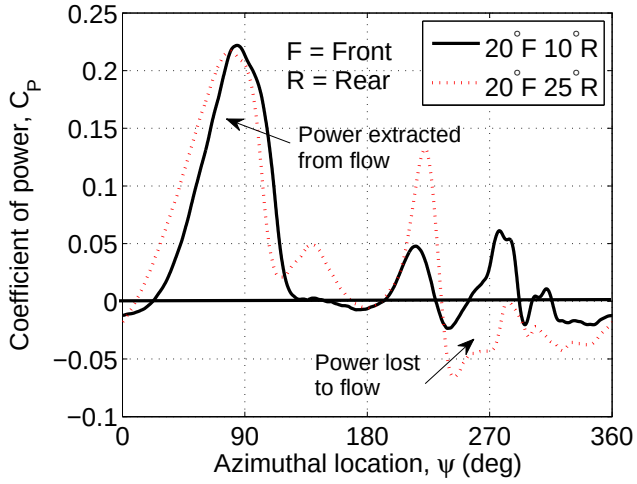

Figure 17: **Variation of coefficient of power (C_P) for one blade as it goes around the azimuth for asymmetric pitching with front pitch angle of 20° and varying rear pitch angles obtained using CFD at TSR=1.2 (positive C_P denotes power extraction and negative C_P is power lost to the flow).**

matics and local wind speed. The only unknown here is the local wind velocity, which could be obtained from the CFD predicted flowfield. Figure 15 shows the CFD predicted flowfield (pressure contours with streamlines superimposed) with relative flow velocities at blade for turbine operating at different blade pitch amplitudes at tip speed ratio (TSR) of 1. Note that, the length and direction of the arrows denoting the different velocity components are proportional to the actual velocity vectors. For the pressure contours, the pressure is normalized with the freestream static pressure or the atmospheric pressure.

It was shown in Fig. 14 that the maximum power extraction occurs in the frontal half especially close to $\Psi = 90°$ and the power loss occurs from $\Psi = 270°$ to $\Psi = 360°$. Therefore, it is important to closely examine the flowfield around the blade and forces experienced by the blade at $\Psi = 90°$ and $\Psi = 270°$. In Fig. 15, the resultant velocity vector at each of these locations were calculated using the blade speed and the CFD-predicted flow velocity. The magnitude and direction of the resultant velocity at the blade is a good indicator of the lift and drag forces experienced by the airfoil and its respective directions. From Fig. 15(a) (pitch amplitude = 15°) it can be seen that at $\Psi = 90°$ the blade is operating at a high angle of attack, probably above stall as indicated by the vortex being shed from the blade. This is the reason for the lower power extracted by the 15° amplitude case as shown in Fig. 14. However, the blade is still producing lift as indicated by the low pressure region (denoted by blue) on top of the airfoil. Also, since the direction of lift is normal to the resultant velocity vector there will be a component of lift in the direction of motion of the blade indicating power capture. Note that the drag force will always have a component opposite to the direction of motion of the blade. At $\Psi = 270°$ the blade is operating at a low angle of attack, however, negative virtual camber (shown in Fig. 11) is stalling the blades and therefore, the lift is probably small and comparable to drag. Even though the lift will have a component in the direction of motion of the blade it will be counteracted by the drag component resulting in a small positive power as shown in Fig. 14. In the case of 20° pitch amplitude (Fig. 15(b)) the magnitude and direction of the resultant velocity at $\Psi = 90°$ is such that the lift and drag is probably similar to the 15° case and hence the power extracted is almost the same. At $\Psi = 270°$, the angle of attack is small, however as in the previous case, because of the negative virtual camber, the component of drag opposite to the direction of blade motion may be balancing out the lift component. From analyzing the flowfield and direction of resultant velocity at $\Psi = 90°$ for the 25° pitch amplitude case (Fig. 24(b)) it can be seen that the angle of attack is low and the blade is unstalled and due to the positive virtual camber (Fig. 11) is producing a large lift force as indicated by the low pressure region on the blade. This shows the significance of blade pitch modulation. For this tip speed ratio a higher pitch angle was required in the front to prevent the blades from stalling. Blade stall was the reason for the lower power capture at $\Psi = 90°$ for the 15° pitch amplitude case. For the 25° pitch amplitude at $\Psi = 270°$, the angle of attack is too low producing very small lift and almost zero power capture. As seen from Fig. 14, the power capture in the front is maximum for the 30° pitch amplitude and the reason for that is similar to the 25° case as seen from Fig. 15(d). At $\Psi = 90°$, the blade operates at an optimal angle of attack, which combined with the positive virtual camber produces significantly large lift. However, at $\Psi = 270°$, the flow scenario is very similar to the previous cases and hence, very small positive power. For the 35° pitch amplitude (Fig. 15(e)), at $\Psi = 90°$, because of the higher pitch angle of the blades, the angle of attack is smaller and hence the lift produced is lower resulting in lower power capture as compared to the 25° and 30° cases. However, at $\Psi = 270°$ the angle of attack is very low but still in same direction as the previous cases, which means, for a symmetric airfoil the direction of lift would be same as the previous cases. However, because of the virtual camber the lift is now in the opposite direction as indicated by the low pressure region on the lower surface of the blade and therefore the component

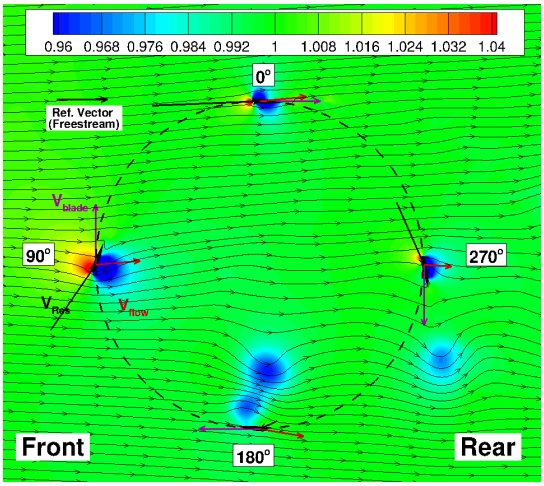

(a) Front pitch = 20°, Rear pitch = 10°.

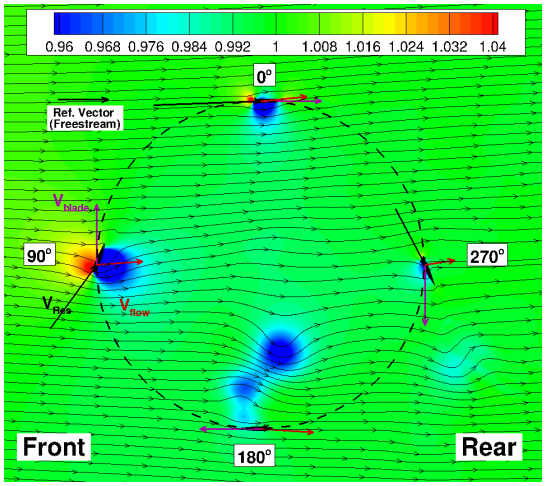

(b) Front pitch = 20°, Rear pitch = 25°.

Figure 18: **Physics of power extraction explained using blade aerodynamics and the CFD predicted flowfield (pressure contours with streamlines superimposed) for turbine operating at front pitch angle of 20° and varying rear pitch angles and tip speed ratio (TSR) of 1.2 (blade chord = 1.3 inches, wind speed = 7 m/s).**

of lift is retarding the blade motion. This is the reason for the negative power at $\Psi = 270°$ as seen from Fig. 14. The 40° pitch amplitude case is shown in Fig. 15(f). It can be seen that at $\Psi = 90°$ the angle of attack is almost zero, but the blade produces a small lift (denoted by the low pressure region on the lower side) because of the positive virtual camber, which helps in the power extraction. However, at $\Psi = 270°$, the angle of attack is zero, but the blade is cambered in such a way that the lift force is opposing the motion of the blade (low pressure region in the lower surface of the blade). This explains the large power loss at this location for the 40° case.

The key insight based on this analysis is that in the frontal half, if the pitch angle is too low (as in the 15° case) the blade would experience very high angle of attack causing the blade to stall. However, if the pitch angle is made very high (35° and 40°) the angle of attack could be very low and even negative which will also reduce the lift and hence power capture. In the rear half of the turbine, very low pitch angle can result in small positive power; however, large angles could cause the lift vector to completely change direction, which will oppose the motion of the blade (negative power). Also, note that the positive virtual camber in the front enhances power capture, however, the negative camber in the rear half causes the blade to stall, which diminishes the amount of power that can be extracted or even lose power back into the flow. In such a case, it might be better to have cambered blades, such that it which would nullify the virtual camber.

Effect of asymmetric blade pitching

The study discussed in the previous section clearly shows the need for dissimilar pitch kinematics in the frontal and rear halves to maximize power extraction. The fundamental reason for this is the fact that the magnitude and direction of the flow velocity at the blade is very different in the front and rear halves. This can be seen from the flow vectors in Fig. 15. Therefore, performance measurements were conducted by keeping the blade kinematics in the frontal half the same and only varying the kinematics in the rear half. Figure. 16(a) shows the measured variation of C_P with tip speed ratio for a range of asymmetric pitch kinematics where the maximum pitch angle in the front was kept at 20° and the maximum pitch angle in the rear half was varied from 5° all the way up to 25° in steps of 5° (blade chord = 1.3 inches). Compared to the symmetric case (20° Front and 20° Rear), reducing the pitch angle in the rear increased efficiency up to 10°. However, decreasing the rear pitch from 10° to 5° significantly reduced efficiency. Also, increasing the rear pitch angle to 25° dramatically reduced power extraction. A similar study was conducted by keeping the max pitch amplitude in the front at 25° and varying the pitch angle in the rear. In this case, as shown in Fig. 16(b), the conclusion was similar to the previous case, which is, decreasing the pitch angle in the rear half improved power extraction.

The next step was to utilize the CFD analysis to analyze the asymmetric pitching cases. Figure 17 shows the variation of CFD-predicted coefficient of power (C_P) for one blade as it goes around the azimuth for

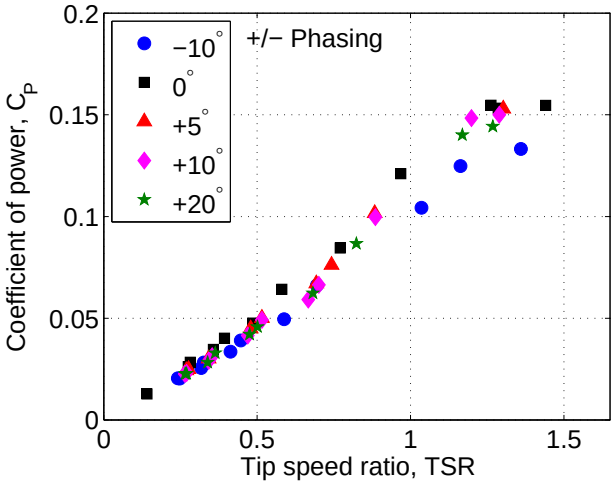

(a) Blade pitch amplitude = 15°.

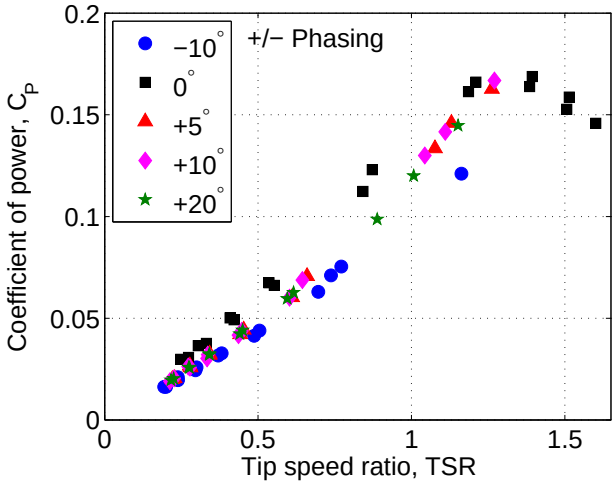

(b) Blade pitch amplitude = 20°.

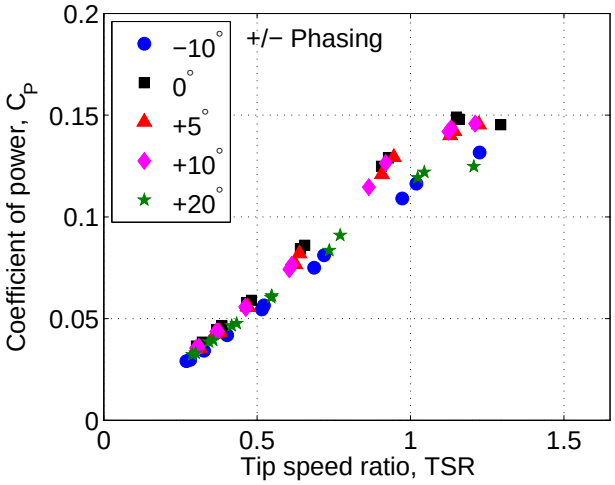

(c) Blade pitch amplitude = 25°.

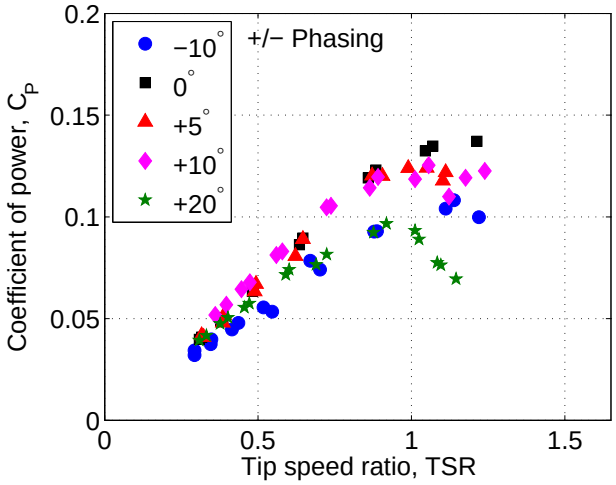

(d) Blade pitch amplitude = 30°.

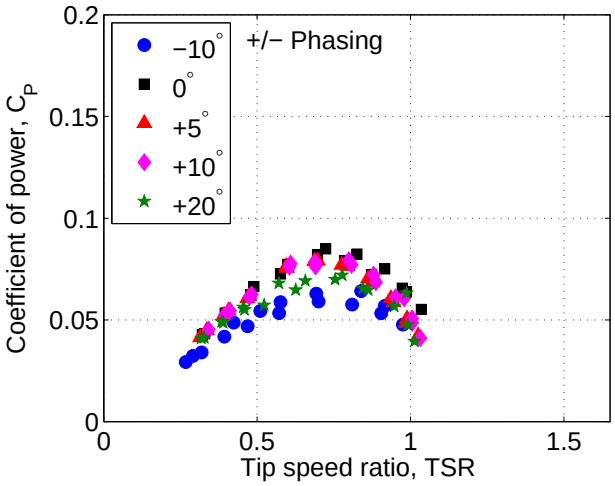

(e) Blade pitch amplitude = 35°.

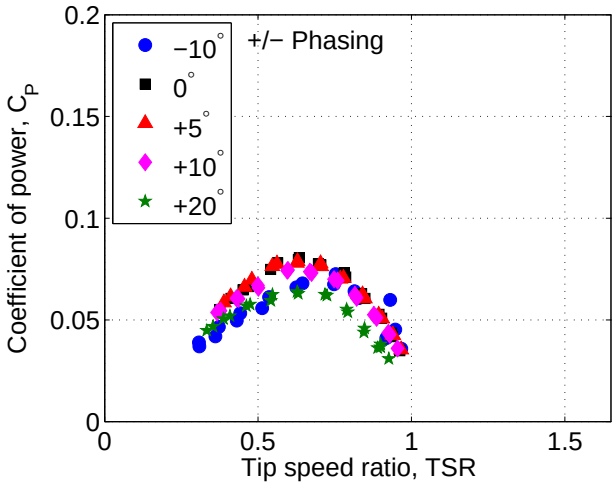

(f) Blade pitch amplitude = 40°.

Figure 19: **Experimental results showing the variation of coefficient of power (C_P) with tip speed ratio (TSR) for phasings of -10°, +5°, +10° and +20° at different blade pitch amplitudes (blade chord = 1.3 inches, wind speed = 7 m/s).**

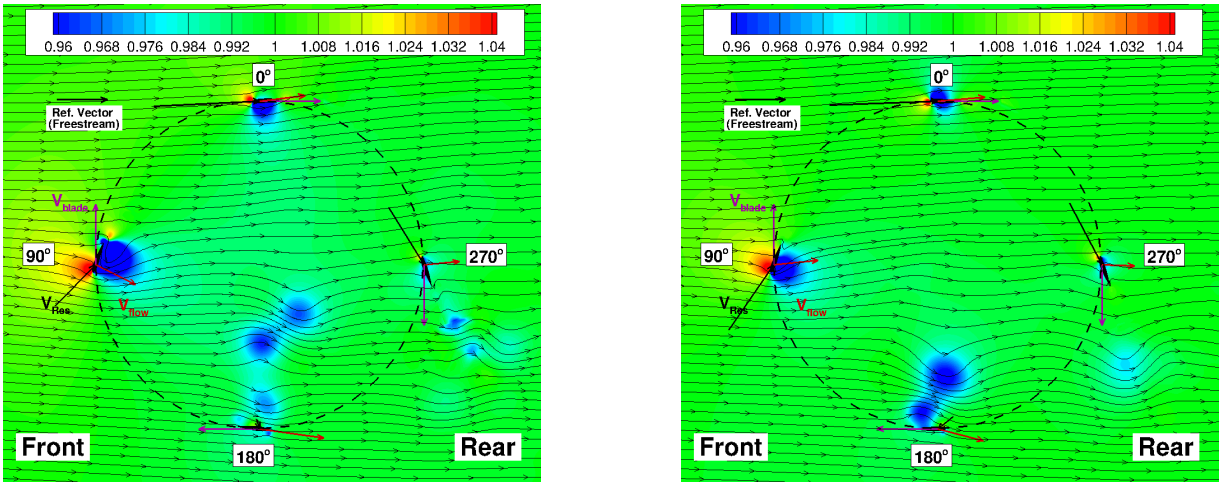

(a) Pitch phasing = +10°.

(b) Pitch phasing = -10°.

Figure 21: **Physics of power extraction explained using blade aerodynamics and the CFD predicted flowfield (pressure contours with streamlines superimposed) for turbine operating at different pitch phasings at a pitch amplitude of 20° and tip speed ratio (TSR) of 1.2 (blade chord = 1.3 inches, wind speed = 7 m/s).**

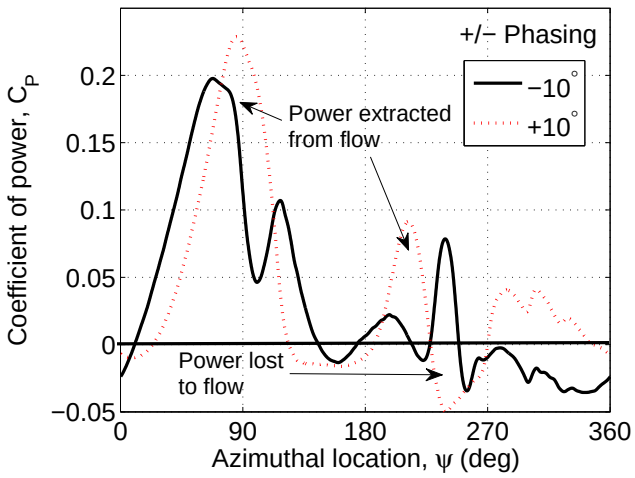

Figure 20: **Variation of coefficient of power (C_P) for one blade as it goes around the azimuth for phasings of -10°, 0°, and +10° at 20° blade pitch amplitude obtained using CFD at TSR=1.2 (positive C_P denotes power extraction and negative C_P is power lost to the flow).**

two different asymmetric pitching cases which are 20°-Front/10°-Rear and 20°-Front/25°-Rear at a tip speed ratio of 1.2. Even though both the asymmetric cases extract almost the same power in the frontal half, most of the power was lost in the rear half for the 25°-Rear case and hence the lower overall performance. The CFD-predicted pressure contours and flowfield given in Fig. 18 can explain the reason for this behavior. Since the interest is in the rear half it is important to focus on $\Psi = 270°$ azimuthal location. For the 10°-Rear case (Fig. 18(a)) at $\Psi = 270°$, it can be seen that because of the small positive angle of attack on the blade, the low pressure region (shown in blue) is on the upper surface of the airfoil. Therefore, in this case the direction of lift has a component in the direction of motion of the blade which is power extraction. This is consistent with Fig. 17, which shows positive power for the 10°-Rear case at $\Psi = 270°$. However, as shown in Fig. 18(b) for the 25°-Rear case at $\Psi = 270°$, the angle of attack is almost zero, but because of the negative virtual camber of the blade the low pressure region is actually on the lower surface of the airfoil which means the direction of lift will oppose the blade motion resulting in power loss. The explains the negative power for 25°-Rear case at $\Psi = 270°$ as seen from Fig. 17. Both experimental and computational study confirms that the optimal pitch kinematics in the frontal half should have a larger blade pitch than the rear half.

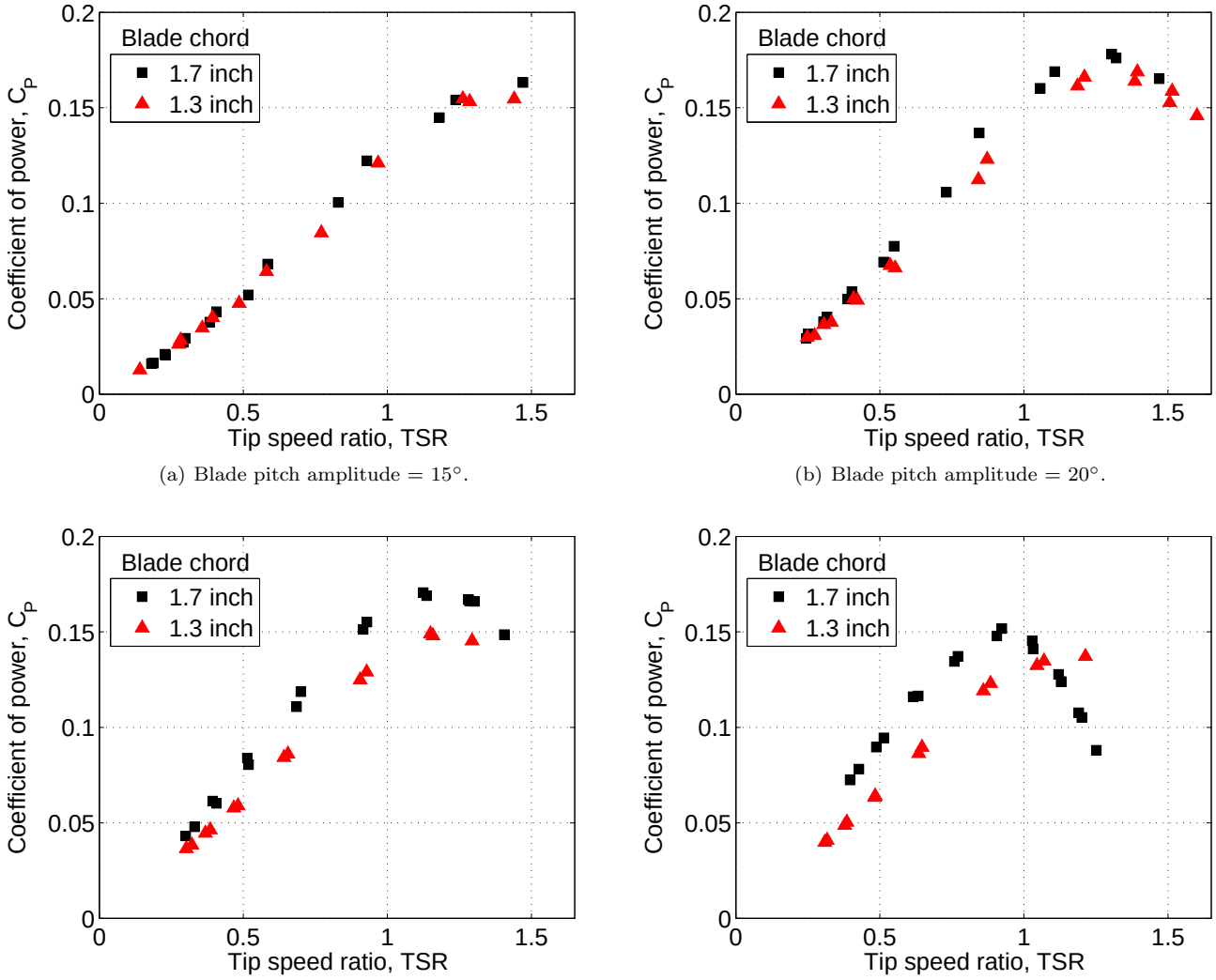

(a) Blade pitch amplitude = 15°.

(b) Blade pitch amplitude = 20°.

(c) Blade pitch amplitude = 25°.

(d) Blade pitch amplitude = 30°.

Figure 22: **Experimental results showing the variation of coefficient of power (C_P) with tip speed ratio (TSR) for two different blade chords at different pitch amplitudes (wind speed = 7 m/s).**

Effect of blade pitch phasing

The next parameter that was varied in the experiments was the phasing of blade pitching with respect to wind direction as denoted by ϕ in Fig. 2. As shown in the figure, changing the phase opposite to the of rotation is positive. In that case the blade attains the maximum pitch angle before $\Psi = 90°$ (phase-lead). Experiments were conducted for a range of pitch amplitudes (symmetric pitching) for phasings of -10°, 0°, +5°, +10°, and +20° (blade chord = 1.3 inches). The results are shown in Fig. 19. Figure 19(a) shows the effect of phasing for 15° pitch amplitude. It is significant to note that a small negative phasing (phase-lag) of 10° greatly reduces efficiency. However, for the positive phasings, the C_P was very similar to the 0° case. The effect of phasing for 20° pitch amplitude is shown in Fig. 19(b). Again, as in the previous case, all the positive phasings have performance very similar to the 0° phasing; however, the efficiency dropped significantly for the -10° phasing. For the 25° and 30° pitch amplitudes (Figs. 19(c) and 19(d)) the trend remained almost the same as the previous cases; however, the efficiency dropped for the +20° phasing also. The same trend remained for the 35° and 40° pitch amplitude cases (Figs. 19(e) and 19(f)); while the 0°, +5° and +10° phasings had similar performance, the +20° and -10° phasings had lower performance. The overall conclusion from the phasing study was that the optimal performance of the turbine is at a phasing of 0°. Also, the performance is forgiving to

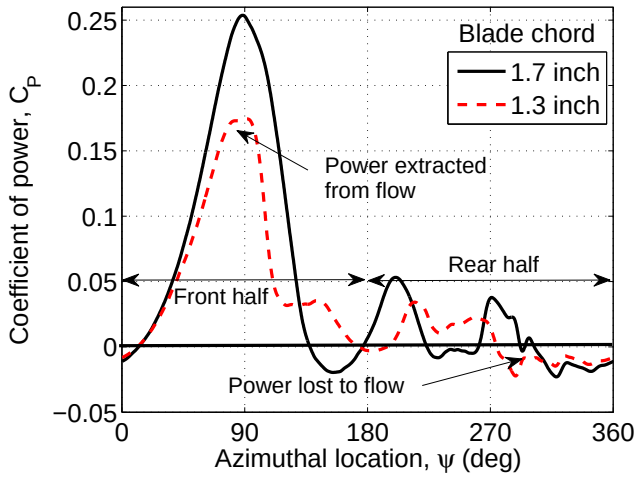

Figure 23: **Variation of coefficient of power (C_P) for one blade as it goes around the azimuth for 1.3 inch and 1.7 inch blade chords at 25° pitch amplitude obtained using CFD at TSR=1.0 (positive C_P denotes power extraction and negative C_P is power lost to the flow).**

small changes in phasing in the positive direction (phase-lead), however, not in the negative direction.

CFD studies were conducted to understand the effect of phasing at the blade aerodynamics level. As in the previous cases, the CFD-predicted coefficient of power (C_P) for one blade as it goes around the azimuth is plotted for two different cases (ϕ = -10° and +10°) at a TSR of 1.2 in Fig. 20. The pitch amplitude is 20° (symmetric pitching) for both the phasings. As seen from the figure higher power extraction in the frontal half occurs for the +10° phasing. Even in the rear half, especially from $\Psi = 270°$ to 360° the +10° case extracts power but the -10° phasing loses power. CFD predicted flowfield shown in Fig. 21 can shed more light into this behavior. Since the biggest difference in power capture is in the frontal half, it is important to look at $\Psi = 90°$ for the -10° and +10° phasings (Figs. 21(a) and 21(b)). Analyzing the flow at $\Psi = 90°$ for the two cases, it can be seen that the blade is producing much higher lift for the 10° lead case ($\phi = +10°$) case than the 10° lag case. Even though the blade pitch angle is almost the same for the two cases at $\Psi = 90°$, the direction of pitching is opposite, which could affect the dynamic lift produced by the blade. More investigation of the unsteady blade aerodynamics would be necessary to understand the reason behind this.

Effect of blade chord

As shown in the previous sections, the virtual camber and incidence (flow curvature effects) of the airfoil plays a crucial role in power extraction. All the previous studies were conducted for a blade chord of 1.3 inches. The chord-to-radius ratio while using the 1.3 inch blade is 0.19 leading to a virtual camber of 2.3% and virtual incidence of 2.7° using a linear approximation. To understand the effect of virtual camber/incidence on power extraction experimental studies were conducted with a blade chord of 1.7 inches which would result in a virtual camber of 3.1% and virtual incidence of 3.6°. Figure 22 shows the comparison between two different blade chords for a range of pitch amplitudes from 15° to 30°. It can be seen that at low pitch amplitudes (15° and 20°) both the blade chords have similar performance. But at higher pitch amplitudes (25° and 30°) the larger blade chord had significantly higher performance. Examining the CFD predicted power by one blade for the the 25° pitch amplitude case (Fig. 23) confirms the larger power extraction by the 1.7 inch blades especially in the frontal half. Comparing the flowfields in Figs. 24(a) and 24(b) clearly shows the larger lift produced on the 1.7 inch chord blades at $\Psi = 90°$ because of the higher positive virtual camber. More studies need to be conducted to obtain the optimal chord/radius ratio for such a turbine.

Summary and Conclusions

The present study focused on utilizing a combined experimental and computational approach to investigate the performance of a dynamic-pitch VAWT, operating at Reynolds numbers of around 15,000 to 20,000. A VAWT prototype with a simplified blade pitch mechanism was designed, built and tested in a wind tunnel. Targeted experiments were conducted to understand the effect of blade pitching amplitude (symmetric pitching), asymmetry in pitch kinematics between frontal and rear halves, and blade chord (or chord/radius ratio) on turbine efficiency. A 2-D CFD model was developed and the model predictions correlated extremely well with experimental data. The validated CFD model was used to develop a fundamental understanding of the effect of the different parameters tested. The following are specific conclusions drawn from this study:

1. Both experimental and CFD studies showed that the turbine efficiency is a strong function of blade pitch kinematics and its phasing. Even though the optimal pitch amplitude is a function of tip speed ratio, moderate pitch amplitudes (± 20°) had the highest overall efficiency for symmetric pitching. The tip speed ratio (TSR) corresponding to the

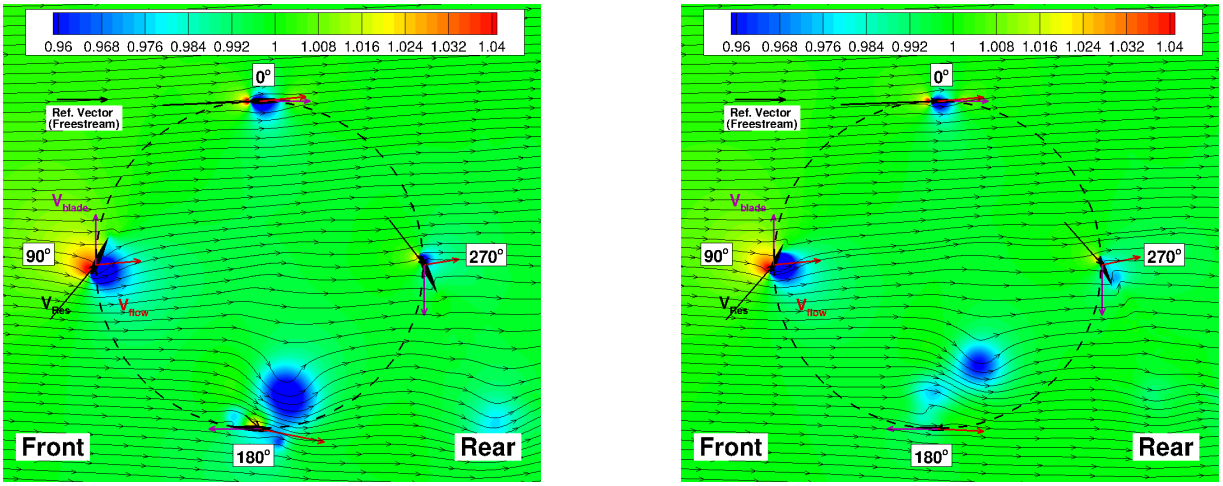

(a) Blade chord = 1.7 inch.

(b) Blade chord = 1.3 inch.

Figure 24: **Physics of power extraction explained using blade aerodynamics and the CFD predicted flowfield (pressure contours with streamlines superimposed) for turbine operating at two different blade chords and pitch amplitude of 20° and tip speed ratio (TSR) of 1.0 (wind speed = 7 m/s).**

maximum C_P decreased with increasing pitch amplitudes. The TSR corresponding to maximum C_P for 20° pitch amplitude was around 1.4, while the optimal TSR for the 40° case was around 0.7. Also, at lower tip speed ratios (TSR<0.8), higher pitch amplitudes have better C_P. The reason for this is, at lower TSRs, because of the lower blade speed, there is more cyclic variation in angle of attack due to the free stream velocity, requiring more modulation in blade pitch angle (higher pitch amplitude) to keep the blade within the optimal operating range and also prevent it from stalling.

2. Experimental studies showed that for maximizing power extraction, the pitch angles required in the front is significantly higher than that in the rear. The reason for this is the decrease in flow velocity between the front and rear halves of the turbine.

3. The optimal performance of the turbine is at a phasing of 0° where the maximum blade pitch occurs at the front ($\Psi = 90°$) and rear ($\Psi = 270°$) locations of the circular blade trajectory. Experiments shows that the performance is forgiving to small changes in phasing (<10°) in the positive direction (phase-lead), however, not in the negative direction (phase-lag).

4. Increasing the chord/radius from 0.19 to 0.25 caused significant improvements in turbine efficiency especially at higher pitch amplitudes. Based on the CFD analysis, the reason for the higher efficiency for the higher chord/radius case is the higher power extraction in the frontal half. This is because, for the larger chord/radius ratio, the virtual camber is higher, which increases the lift produced in the front and hence the power extracted.

5. A general insight gained from the computational study is that the blade extracts most of the power in the frontal half, however, captures very minimal power in the rear half. In the frontal half, if the pitch angle is too low the blade would experience very high angle of attack causing the blade to stall. However, if the pitch angle is made very high the angle of attack could be very low and even negative which will also reduce the lift and hence power capture. In the rear half of the turbine, very low pitch angle can result in small positive power; however, large angles could cause the lift vector to completely change direction, which will oppose the motion of the blade (negative power). Also, the positive virtual camber in the front enhances power capture, however, the negative camber in the rear half causes the blade to stall, which diminishes the amount of power that can be extracted or even lose power back into the flow. In such a case, it might be better to have cambered blades, such that it which would nullify the virtual camber. Also, it should be noted that, the reason for the lower overall measured C_P values is the lower operating Reynolds numbers of the present experimental prototype.

.

REFERENCES

[1] Kirke, B. K., "Evaluation of Self-Starting Vertical Axis Wind Turbines For Stand-Alone Applications," Ph.D Thesis, School of Engineering, Griffith University Gold Coast Campus, April 1998.

[2] Dabiri, J. O., "Potential order-of-magnitude enhancement of wind farm power density via counter-rotating vertical-axis wind turbine arrays," *Journal of Renewable and Sustainable Energy*, Vol. 3, 2011, pp. 043104-1 – 043104-12.

[3] McGowan, R., Lozano, R., Raghav, V., and Komerath, N., "Vertical Axis Micro Wind Turbine Design for Low Tip Speed Ratios, "Proceedings of the 3rd International Multi-Conference on Complexity, Informatics and Cybernetics," Orlando, FL, March 25 – 28, 2012.

[4] Parashivoiu, I., and Delclaux, F., "Double Multiple Streamtube Model with Recent Improvements," *Journal of Energy*, Vol. 7, No. 3, May – June 1983, pp. 250 – 255.

[5] Parashivoiu, I., Trifu, O., and Saeed, F., "H-Darrieus Wind Turbine with Blade Pitch Control," *International Journal of Rotating Machinery*, Vol. 2009, 2009, pp. 1 – 7.

[6] Asher, I. M., Drela, M., and Peraire, J., "A Low Order Model for Vertical Axis Wind Turbines," Proceedings of the 28th AIAA Applied Aerodynamics Conference, Chicago, IL, June 28 – July 1, 2010.

[7] Benedict, M., Lakshminarayan, V. K., Johnathan, P., and Chopra, I., "Fundamental Understanding of the Physics of a Small-Scale Vertical Axis Wind Turbine with Dynamic Blade Pitching: An Experimental and Computational Approach," Proceedings of the 54th AIAA/ASME/ASCE/AHS/ASC Structures, Structural Dynamics, and Materials Conference, Boston, Massachusetts, April 8 – 11, 2013.

[8] Lakshminarayan, V. K., "Computational Investigation of Micro-Scale Coaxial Rotor Aerodynamics in Hover," Ph.D. dissertation, Department of Aerospace Engineering, University of Maryland at College Park, 2009.

[9] Pulliam, T., and Chaussee, D., "A Diagonal Form of an Implicit Approximate Factorization Algorithm," *Journal of Computational Physics,* Vol. 39, (2), February 1981, pp. 347–363.

[10] Van Leer B., "Towards the Ultimate Conservative Difference Scheme V. A Second-Order Sequel To Godunovs Method, *Journal of Computational Physics*, Vol. 135, No. 2, 1997, pp. 229-248.

[11] Roe, P., "Approximate Riemann Solvers, Parameter Vectors and Difference Schemes," *Journal of Computational Physics*, Vol. 135, No. 2, 1997, pp. 250-258.

[12] Koren, B., "Multigrid and Defect Correction for the Steady Navier-Stokes Equations", Proceedings of the 11th International Conference on Numerical Methods in Fluid Dynamics , Willamsburg, VA, June 1988.

[13] Turkel, E., "Preconditioning Techniques in Computational Fluid Dynamics," *Annual Review of Fluid Mechanics,* Vol. 31, 1999, pp. 385–416

[14] Spalart, P. R., and Allmaras, S. R., "A One-equation Turbulence Model for Aerodynamic Flows," AIAA Paper 1992-0439, 30th AIAA Aerospace Sciences Meeting and Exhibit, Reno, NV, January 6–9, 1992.

[15] Lee, Y., "On Overset Grids Connectivity and Automated Vortex Tracking in Rotorcraft CFD," Ph.D. Dissertation, Department of Aerospace Engineering, University of Maryland at College Park, 2008.

[16] Migliore, P. G., Wolfe, W. P., and Fanuccif, J. B., "Flow Curvature Effects on Darrieus Turbine Blade Aerodynamics," *Journal of Energy*, Vol. 4, (2), 1980, pp. 49–55

[17] Benedict, M., "Fundamental Understanding of the Cycloidal-Rotor Concept for Micro Air Vehicle Applications," Ph.D Thesis, Department of Aerospace Engineering, University of Maryland College Park, December 2010.